Energy transfer efficiency in YF_3 nanocrystals: Quantifying the Yb^{3+} to Tm^{3+} infrared dynamics

Marta Quintanilla,[1,a)] Nuria O. Núñez,[2] Eugenio Cantelar,[1] Manuel Ocaña,[2] and Fernando Cussó[1]
[1]*Universidad Autónoma de Madrid, Departamento de Física de Materiales (C-IV), Avda. Francisco Tomás y Valiente 7, 28049 Madrid, Spain*
[2]*Instituto de Ciencia de Materiales de Sevilla, CSIC-US, Américo Vespucio 49, 41092 Isla de la Cartuja, Seville, Spain*

(Received 8 November 2012; accepted 15 April 2013; published online 7 May 2013)

In this work, we report on the determination of the infrared $Yb^{3+} \rightarrow Tm^{3+}$ energy transfer efficiency in YF_3:Yb^{3+}/Tm^{3+} nanocrystals through the study of Yb^{3+} dynamics. The obtained results are compared to those previously reported in macrocrystals to analyze possible changes related to size reduction. Luminescence lifetimes are much shorter in the nanoparticles than in bulk samples, a behavior that can be related to $Yb^{3+} \rightarrow Yb^{3+}$ migration and the enhanced surface/volume ratio of the nanoparticles. On the other hand, $Yb^{3+} \rightarrow Tm^{3+}$ energy transfer macroparameter remains unaltered, demonstrating that spectroscopic intrinsic parameters such as radiative and non-radiative probabilities are not affected by size reduction. Finally, a formula that describes Yb^{3+} lifetime dependence with Yb^{3+} and Tm^{3+} concentration is proposed, considering both the effects produced by migration between Yb^{3+} ions and energy transfer from Yb^{3+} to Tm^{3+} ions. [http://dx.doi.org/10.1063/1.4803540]

I. INTRODUCTION

Infrared-to-visible upconversion (UC) in rare-earth (RE) based phosphors has been extensively studied during the last decades because of their wide and important applications, including color displays[1,2] and solid-state lasers.[3–5] Recently, the interest is renewed because of the potential application of RE-doped nanosized materials in bioimaging techniques.[6–8] Compared to the traditional biological labels, such as organic dyes and semiconductor nanoparticles, RE-based nanoparticles possess several inherent advantages, including weak auto-fluorescence background, excitation at *near-infrared* (NIR), where a strong penetration in tissues is found, resistance to photobleaching, and low toxicity.[9–12]

Among the different hosts available, fluoride materials outstand due to the high efficiency of UC processes that can be achieved, which can be related to their relatively low lattice phonon energy. In particular, YF_3 sensitized by Yb^{3+} ions and activated by Tm^{3+} ions exhibit very efficient upconverted visible and near-UV emissions that are being widely studied.[13–17]

The accessibility to nanocrystals' synthesis routes that can provide narrow size distributions and morphological homogeneity allows researching the effects of size and shape in the luminescence properties of the material. Concerning YF_3 co-doped with Yb^{3+} and Tm^{3+}, most of the synthesis routes proposed in the literature led to irregular particles in the nano- or micrometer range, and only two proposals led to truly uniform nanocrystals[15,18] that could be applied to study size-dependant properties.

Most of the studies that consider size as a variable attribute the differences of the upconverted intensities to surface defects (due to the increased surface/volume ratio in the nanoparticles compared to volume samples) or to the confinement of phonons, which could modify the non-radiative transition and non-resonant energy transfer probabilities.[19–24] These studies have improved the knowledge of the phenomenology involved in the UC emissions, but very little attention has been devoted to the luminescence dynamics and to the quantification of the physical magnitudes that describe energy transfer in the nanocrystals. In particular, energy transfer parameters, which represent the probability of the processes, have not been determined yet, although they would provide a deeper comprehension of the phenomena and would establish whether there are important spectroscopic differences in comparison to the bulk material.

In this work, we report on the determination of the IR energy transfer macroparameter in YF_3:Yb^{3+}/Tm^{3+} nanocrystals and we compare our results with those previously obtained in macrocrystals.

II. EXPERIMENTAL METHOD

YF_3 nanoparticles doped with different concentrations of Yb^{3+} or Yb^{3+}/Tm^{3+} ions were synthesized using the procedure described elsewhere:[25] proper amounts of RE precursors (yttrium(III) acetate, Aldrich 99.9%; thulium(III) acetylacetonate, Alpha Aesar 99.9%; and ytterbium(III) acetylacetonate, Alpha Aesar 99.9%) were dissolved in ethylene glycol (Fluka, 99.5%) under magnetic stirring at ~100 °C to facilitate the dissolution process. These solutions were cooled down to room temperature and then the desired volume of ionic liquid [BMIM]BF_4 (Fluka, 97%) was admixed keeping the magnetic stirring. The final solutions were then aged for 15 h in tightly closed test tubes using an oven preheated at ~120 °C.

a)marta.quintanilla@uam.es

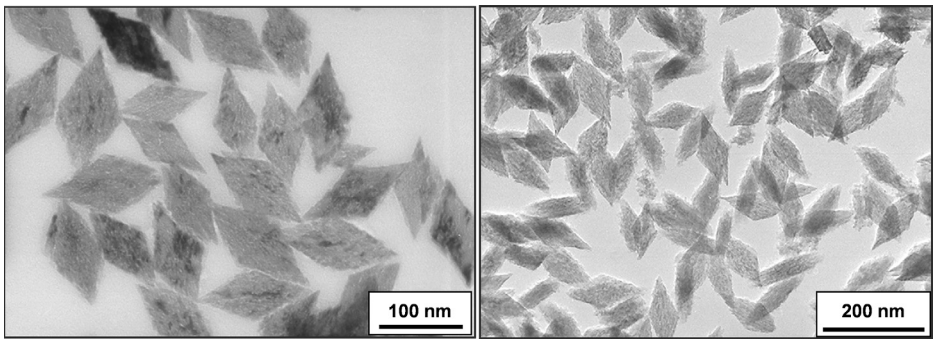

FIG. 1. TEM micrographs of $[Tm^{3+}] = 2$ mol. % and $[Yb^{3+}] = 20$ mol. % nanocrystals, where the high homogeneity of the sample and the rhombic shape can be appreciated.

After ageing, the resulting dispersions were cooled down at room temperature, centrifuged to remove the supernatants, and washed in ethanol and distilled water. The powders were then dried at 50 °C and annealed for 20 min at 400 °C. This procedure has been proved to be adequate to eliminate residual OH^- groups, resulting in enhanced fluorescence properties, while preserving the size and shape of the nanocrystals.[26]

The morphological and structural characterizations of the nanoparticles have been reported elsewhere.[15] In that work, it was shown that they crystallized into the orthorhombic YF_3 structure and show a highly homogeneous chemical composition. They also present rhombic shape (Figure 1) and a mean size of 125 × 55 × 23 nm, a data obtained from TEM micrographs by counting several hundreds of particles.

The optical characterization has been performed under diode laser excitation (LIMO) at 975 nm. The luminescence of the powdered samples has been dispersed and selected with a monochromator (ARC Spectrapro 500-I) and then detected with a photomultiplier tube (PMT) (Thorn Emi QB9558) for the visible range or an InGaAs photodiode (Hamamatsu P8079) for the near-IR range.

III. RESULTS AND DISCUSSION

The infrared emission of Yb^{3+} ions is shown in Figures 2(a) and 2(b) for single doped samples and for samples co-doped with Tm^{3+} ions, respectively. In the case where only Yb^{3+} ions are present, the intensity of the emission in the samples is lower at higher concentrations. This behavior could be related to migration between Yb^{3+} ions, an effect that will be analyzed later. On the other hand, in the codoped samples, the emission intensity decreases when Tm^{3+} ions concentration is increased keeping constant Yb^{3+} content. To understand this, it has to be considered that there are energy transfer processes involving these ions that will modify the population density in the different excited states. As an example, in the inset of Figure 2(b), the visible and UV upconverted luminescence of YF_3:Yb^{3+}/Tm^{3+} nanoparticles after selective CW excitation of Yb^{3+} ions at 975 nm is shown. All the observed emissions are distinctive of Tm^{3+} ions and confirm with their presence the existence of energy transfer and UC mechanisms involving Yb^{3+} and Tm^{3+} ions. The transitions associated with the different emission bands are labeled in the figure. According to the traditionally accepted description of the energy transfer in Yb^{3+}/Tm^{3+} co-doped materials, the different energy levels of Tm^{3+} ions are populated through a chain of at least three consecutive energy transfer processes from Yb^{3+} ions.[27,28] These processes are schematically depicted in Figure 2(c).

As it can be seen, once Yb^{3+} ions are populated, a first energy transfer step from Yb^{3+} to Tm^{3+} can take place ($^2F_{5/2}$ → $^2F_{7/2}$ (Yb^{3+}):$^3H_6$ → $^3H_5$ (Tm^{3+})), followed by a non-radiative relaxation from $^3H_5$ level that populates the lower

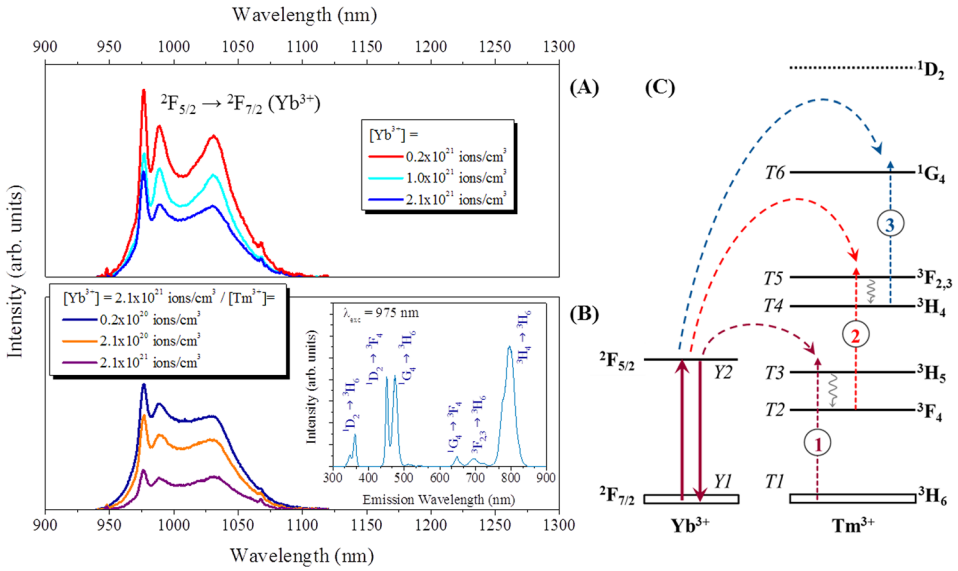

FIG. 2. (a) Emission spectra of Yb^{3+} ions in YF_3:Yb^{3+} single doped nanoparticles. (b) Emission spectra of Yb^{3+} ions in Yb^{3+}/Tm^{3+} doped YF_3 nanoparticles. In the inset, it is shown the emission spectrum in the UV and VIS ranges of $[Tm^{3+}] = 2$ mol. % and $[Yb^{3+}] = 20$ mol. % sample under excitation at 975 nm. (c) Yb^{3+} → Tm^{3+} energy transfer processes. The dashed arrows stand for the three processes involved. The nomenclature used to label the levels in the rate equations is also included.

lying excited level of thulium ($^3F_4$). Then, a second energy transfer from Yb^{3+} ions ($^2F_{5/2} \rightarrow {}^2F_{7/2}$ (Yb^{3+}):$^3F_4 \rightarrow {}^3F_{2,3}$ (Tm^{3+})) populates $^3F_{2,3}$ level of Tm^{3+} ions. $^3F_{2,3}$ can be also relaxed following a non-radiatively path that now will populate $^3H_4$ level. Later, it is possible to observe a third upconversion process from Yb^{3+} that populates $^1G_4$ level ($^2F_{5/2} \rightarrow {}^2F_{7/2}$ (Yb^{3+}):$^3H_4 \rightarrow {}^1G_4$ (Tm^{3+})). A further step to populate an even higher energy level of thulium, $^1D_2$, also takes place; although in this case the exact mechanism is not yet fully elucidated and different possibilities are usually considered.[16,29–31]

As it can be deduced from Figure 2(c), the probability of the second and third upconversion processes depends on the probability of the first IR energy transfer from Yb^{3+} ions to Tm^{3+} ions, which triggers all the subsequent steps. Therefore, the first energy transfer mechanism is the key process to allow the upconversion, and any change in that process will strongly affect the intensity of the visible and UV emissions.

The population dynamics and the emission of the different Yb^{3+} and Tm^{3+} levels in macroscopically sized YF_3 crystals have been described in a classical paper by Ostermayer *et al.*[27] Nevertheless, it was demonstrated that while the first up-conversion step can be accurately characterized, the quantitative evaluation of the second and third ones is not so straightforward.[27,32] Considering all these facts, we will focus our attention in the quantification of the first energy transfer step probability.

Using a set of coupled differential rate equations, macroscopic energy transfer coefficients (K_i) can be used to quantify energy transfer probabilities.[27] After selective Yb^{3+} excitation, the dynamics of the ytterbium excited state ($^2F_{5/2}$) can be expressed (applying the notation for the energy levels shown in Figure 2(c)) as

$$\frac{dN_{Y2}}{dt} = \sigma_{abs}\phi N_{Y1} - (A_{Y21} + W_{Y21}^{NR})N_{Y2} - K_1 N_{Y2} N_{T1} - K_2 N_{Y2} N_{T2} - K_3 N_{Y2} N_{T4}, \quad (1)$$

where σ_{abs} is the Yb^{3+} absorption cross section, ϕ is the excitation photon flux and N_{Yi} (i = 1, 2) and N_{Tj} (j = 1,…, 6) represent the population densities (in ions/cm^3) of the different ytterbium and thulium levels, respectively. Transition rates are expressed in terms of the radiative, A_i, and non-radiative, W^{NR}, decay rates, while K_i (i = 1, 2, 3) are the macroscopic transfer parameters associated to each $Yb^{3+} \rightarrow Tm^{3+}$ energy transfer.

Following the paper by Ostermayer *et al.*,[27] the first parameter K_1 can be deduced from the dependence of Yb^{3+} lifetime on Tm^{3+} concentration. After pulsed excitation, the populations of the upper levels become negligible, as it is the back-transfer process from Tm^{3+} to Yb^{3+} due to the relatively high energy mismatch between the donor and acceptor transitions (~1650 cm^{-1}). Thus, Eq. (1) can be simplified and then written in terms of decay time to have

$$\frac{1}{\tau_{exp}} = \frac{1}{\tau_{Y2}} + K_1 N_{T1}, \quad (2)$$

where τ_{exp} is the measured decay time and τ_{Y2} is the lifetime of the Yb^{3+} excited state in the absence of energy transfer to Tm^{3+} ions. It can be inferred from Eq. (2) that Yb^{3+} ions will exhibit a lifetime that decreases linearly with Tm^{3+} concentration. This simple relationship between both magnitudes can be used to determine the energy transfer coefficient K_1 which, as previously stated, is the most basic parameter describing Yb^{3+} to Tm^{3+} interactions.

For that reason, lifetime measurements, after selective pulsed excitation of Yb^{3+} ions ($\lambda_{exc} = 975$ nm), have been performed in samples with variable thulium content ([Tm^{3+}] ranging from 0.1 mol. % up to 10 mol. %) and constant ytterbium concentration at [Yb^{3+}] = 10 mol. % (2.1×10^{21} ion/cm^3).[15] To avoid any laser background, the lifetimes have been measured at 1030 nm, where Yb^{3+} ions show the furthest emission peak from the excitation laser (Figures 2(a) and 2(b)). The obtained results are presented in Figure 3.

As it can be observed, the decays are non-exponential. Energy transfer processes can sometimes (depending on the probability of the different processes involved[33]) account for divergences from a purely exponential behavior, as it is often the case in Yb^{3+}/Tm^{3+} systems.[27] Also, in the special case of nano-emitters, non-exponential behaviors such as those observed in Figure 3 can be also attributed to the enhanced weight of surface defects on the decay curves in comparison to those obtained in bulk materials due to the high surface/volume rate.[34] Therefore, it can be assumed that both effects are taking place in our case.

The lifetimes of lanthanide ions affected by energy transfer processes are generally described by the classical formalism of Inokuti-Hirayama or alternatively, Yokota-Tanimoto.[35,36] Nevertheless, in the present case, as it has been mentioned before, the high surface/volume ratio is likely to modify the shape of the decay curves and, thus, this formalism cannot be applied. For this reason, different criteria to quantify the lifetimes of nanoparticles can be found in the literature.[24,34,37–40] Here, in order to facilitate the comparison to the data previously published for YF_3 crystals, we shall adopt the criteria used by Ostermayer *et al.*[27] and quantify Yb^{3+} lifetimes using the time to decay to I/e, where I is

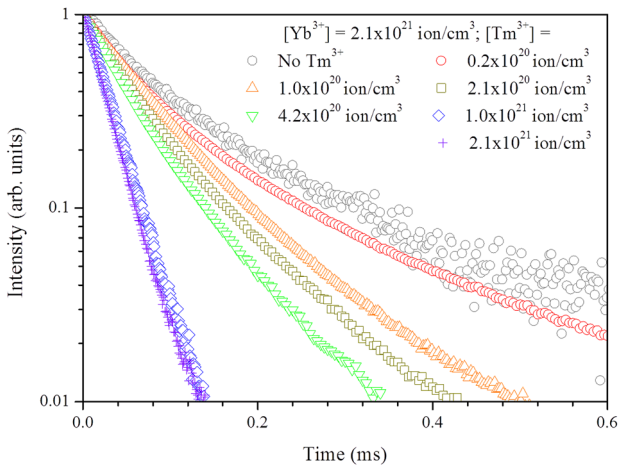

FIG. 3. Temporal evolution of the Yb^{3+} luminescence ($^2F_{5/2} \rightarrow {}^2F_{7/2}$ transition) as function of the Tm^{3+} content.

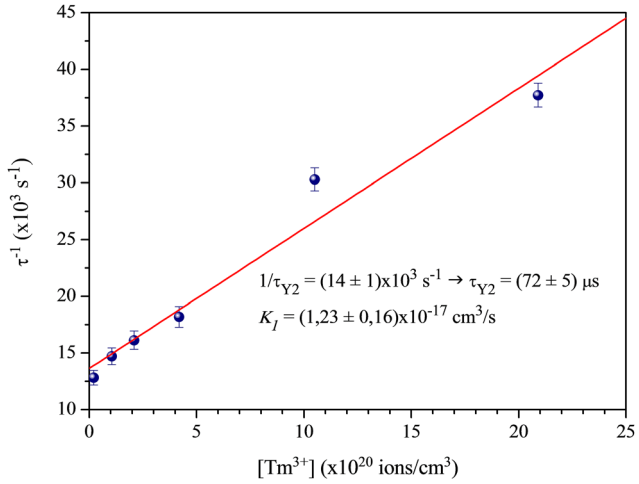

FIG. 4. Dependency of $^2F_{5/2}(Yb^{3+})$ lifetime with Tm^{3+} concentration. The line is the least square fitting of the experimental data.

the initial intensity. The inverse of the measured lifetimes for nanocrystals with $[Yb^{3+}] = 10$ mol. % and variable $[Tm^{3+}]$ is represented in Figure 4 as function of Tm^{3+} concentration. According to the figure, the results follow the expected linear dependence predicted by Eq. (2). From the least square fitting of the experimental data, an energy transfer coefficient $K_1 = (1.2 \pm 0.2) \times 10^{-17}$ cm^3/s and an intrinsic lifetime of Yb^{3+} ions at the present concentration $\tau_{Y2} = (72 \pm 5)$ μs are obtained.

These values for K_1 and τ_{Y2} can be now compared to those previously calculated by Ostermayer *et al.*[27] for polycrystalline YF_3 crystals with macrometric sizes: $K_1 = 1.2 \times 10^{-17}$ cm^3/s and $\tau_{Y2} = 1650$ μs. For clarity, in Figure 5, the measured values of $^2F_{5/2}(Yb^{3+})$ lifetime are plotted together with those obtained by Ostermayer *et al.*[27]

It is clear that Yb^{3+} lifetimes in the absence of energy transfer (low Tm^{3+} content limit) are substantially lower in the nanoparticles than in the polycrystalline material; however, the transfer coefficient has the same value in both cases. The coincidence of the transfer rate between macroscopic samples and nanoparticles can be understood considering the spectroscopic physical meaning of the magnitude. The macroscopic energy transfer parameter, K_1, is directly related to the ion-ion interaction between ytterbium and thulium ions,[41–43] and therefore, to the microscopic parameter describing $Yb^{3+} \rightarrow Tm^{3+}$ interaction, which exclusively depends on intrinsic spectroscopic magnitudes such as absorption and radiative and non-radiative probabilities.[44] These intrinsic parameters are not expected to suffer modifications as long as the material preserves characteristics such as crystal structure, lattice parameters, and optical center distribution, which seem to be the same in the crystals and nanoparticles. Therefore, the relevant differences obtained in the two different kinds of samples must be related to a different effect.

It is clear from Figure 5 that energy transfer processes in polycrystalline samples start competing with the Yb^{3+} intrinsic decay at Tm^{3+} concentrations of 2×10^{19} ions/cm^3 ($\sim$0.1 mol. %), while in the nanoparticles, this effect becomes significant only above $[Tm^{3+}] = 2 \times 10^{20}$ ions/cm^3 ($\sim$1 mol. %). This difference is related to the variation observed for the "intrinsic" Yb^{3+} lifetime, τ_{Y2}, that is, without Tm^{3+}. Being the effect of Tm^{3+} ions excluded, the only difference between the two different kinds of samples has to be related to $Yb^{3+} \rightarrow Yb^{3+}$ energy transfer, also known as migration, which can be very efficient and gives rise to self-quenching.

To analyze the self-quenching related to Yb^{3+} content, new series of single doped Yb^{3+}:YF_3 nanoparticles were prepared, with concentrations ranging from 1 mol. % up to 10 mol. %. The luminescence decays, measured in the same conditions applied before, are presented in Figure 6. It can be observed that, again, the decays are non-exponential and become faster as Yb^{3+} concentration increases.

The dependence of the lifetime with Yb^{3+} concentration in terms of I/e of the decay time is shown in Figure 7. According to the results, τ^{-1} follows a linear dependence with Yb^{3+} concentration, indicating a clear self-quenching

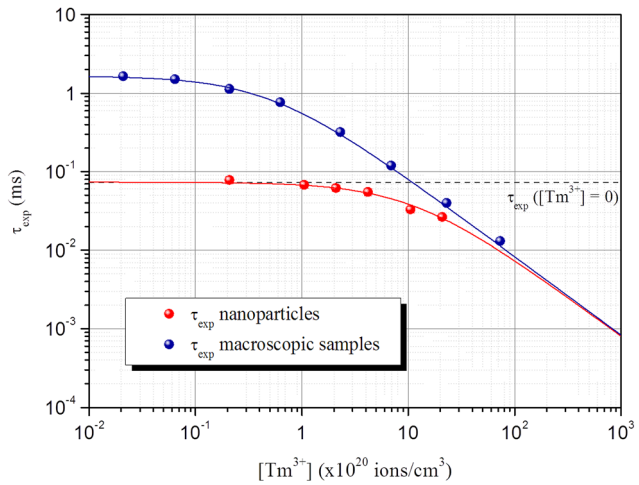

FIG. 5. Experimental lifetime values obtained for YF_3:Yb^{3+}/Tm^{3+} nanoparticles for different Tm^{3+} contents and data obtained by Ostermayer *et al.*[27] For the sake of clarity, in the case of nanoparticles, the lifetime obtained when no Tm^{3+} ions are present (intrinsic Yb^{3+} lifetime) is added as a dashed line.

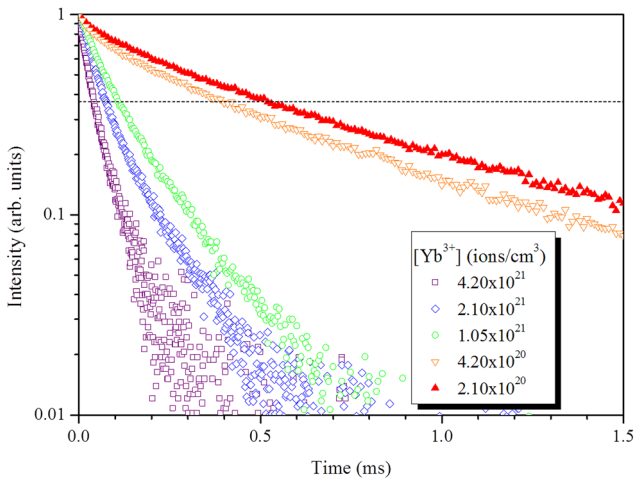

FIG. 6. Temporal decay of $^2F_{5/2}(Yb^{3+})$ luminescence in samples with variable Yb^{3+} content and without Tm^{3+} ions.

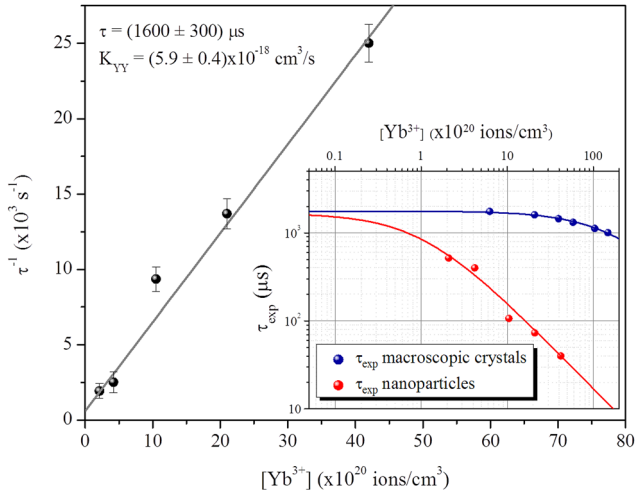

FIG. 7. Experimental lifetime variation of $^2F_{5/2}(Yb^{3+})$ with Yb^{3+} concentration (without thulium ions). The least square fitting of τ^{-1} vs. $[Yb^{3+}]$ is plotted to determine K_{YY} and τ_Y, and the curved obtained with the fit is shown in the inset.

associated to Yb^{3+} ions. As it has been done before, the self-quenching can be described as

$$\frac{1}{\tau_{exp}(Yb^{3+})} = \frac{1}{\tau_{Yb}(0)} + K_{YY}N_{Yb}, \tag{3}$$

where $\tau_{exp}(Yb^{3+})$ represents the measured decay time for different Yb^{3+} concentrations, and K_{YY} represents a macroscopic parameter related to the probability of all the concentration dependent mechanisms that could depopulate ytterbium ions. The experimental data can be fitted (continuous grey line in Figure 7) to obtain $K_{YY} = (5.9 \pm 0.4) \times 10^{-18}$ cm^3/s and $\tau_{Yb}(0) = (1600 \pm 300)$ μs.

As it can be seen, the macroparameter related to migration between Yb^{3+} ions (K_{YY}) is an order of magnitude lower than the corresponding parameter for Yb^{3+} to Tm^{3+} energy transfer, K_1. Nevertheless, it has a sizeable effect on the observed lifetimes and accounts for some reduction on them. Substituting the calculated K_{YY} and $\tau_{Yb}(0)$ values in Eq. (3), a curve representing the lifetime of Yb^{3+} ions (red line in the inset of Figure 7) can be calculated, and it shows that some migration effect is observed even in the sample with the lowest Yb^{3+} concentration considered.

It is clear that energy migration facilitates the excitation light to travel through the material and eventually to reach quenchers such as vacancies and impurities that could reduce the lifetime. Generally, the material surface is expected to have a relatively high amount of defects, and therefore, in materials such as nanoparticles that have a large surface/volume ratio, especially when there are no further coatings, as it is the case, self-quenching related to high $Yb^{3+} \rightarrow Yb^{3+}$ energy migration is expected.

Once again, it is possible to compare the lifetimes obtained for Yb^{3+} ions in the nanoparticles to those obtained by Ostermayer *et al.*[27] using macroscopic crystals doped with different Yb^{3+} concentrations. The comparative graph is shown in the inset of Figure 7. It is clear that the difference between the lifetimes measured for the nanoparticles and for the macroscopic crystals is larger for larger Yb^{3+} concentrations. On the contrary, for lower Yb^{3+} contents, both fitted curves tend to approximately the same value that, in fact, can be assumed to be the same one taking into account the error of the linear fitting in Figure 7. This result is consistent with the formerly exposed effect of surface quenchers on the lifetimes after energy migration through Yb^{3+} ions. First, this effect would be larger at higher Yb^{3+} concentrations, since energy migration is favored in that case and second, the effect would be stronger in nanoparticles than in macroscopic crystals, since the surface/volume ratio is much larger for the nanoparticles. Consequently, it can be assumed that the main reason behind the shorter lifetimes in the nanoparticles, which was first observed in Figure 5, is the presence of quenchers on their surface.

Looking at Figure 5 and at the inset of Figure 7, it can be observed that the comparison between nanoparticles and macroscopic samples follows exactly the opposite behavior in each case. In Figure 5, the lifetimes at low dopant concentration are more than one order of magnitude different, while in Figure 7 they are the same. On the other hand, K_i does not change for $Yb^{3+} \rightarrow Tm^{3+}$ interaction, while it is strongly affected in the $Yb^{3+} \rightarrow Yb^{3+}$ study. To understand these results, it has to be considered that the studied effects are different in each case. In the first situation (Figure 5), Tm^{3+} concentration is being changed and Yb^{3+} lifetimes are used as a probe. Therefore, energy migration between Yb^{3+} ions will always be the same and the only reason that could modify the lifetimes is $Yb^{3+} \rightarrow Tm^{3+}$ interaction.

On the contrary, for the $Yb^{3+} \rightarrow Yb^{3+}$ study, the measured lifetime is the one associated to the ion which concentration is being modified. Consequently, K_{YY} parameter would account not only for energy transfer between two Yb^{3+} ions (migration) but also for the effect of quenchers on the acceptor ion, being this the reason why K_{YY} is different in nanoparticles and in macroscopic samples. This also explains why at lower Yb^{3+} contents the lifetime in both kinds of samples is the same.

Therefore, as it has been proved, the $^2F_{5/2}$ temporal evolution is affected by the energy transfer to the acceptor ions ($Yb^{3+} \rightarrow Tm^{3+}$) as well as by migration between donor ions ($Yb^{3+} \rightarrow Yb^{3+}$). Considering the previous results, τ_{exp} can be expressed in one single relationship as

$$\frac{1}{\tau_{exp}} = \frac{1}{\tau_{Yb(0)}} + K_1'N_{Tm} + K_{YY}N_{Yb}, \tag{4}$$

where $K_{YY} = 5.9 \times 10^{-18}$ cm^3/s and $\tau_{Yb(0)} = 1600$ μs. According to Mita *et al.*,[32] in the low concentration regime the transfer parameter K_1' has an initial dependence on Yb^{3+} content and it tends to K_1 for sufficiently high Yb^{3+} concentrations. Therefore, it can be expressed as $K_1' = 1.23 \cdot 10^{-17}\{1 - \exp(-8 \cdot 10^{-22}N_{Yb})\}$.

Summarizing, it has been observed that from the microscopic point of view, there is no change on the energy transfer probabilities comparing bulk crystals with nanoparticles. Nonetheless, migration effects become much stronger in the second case, effectively shortening the lifetimes of Yb^{3+}

ions. In Yb^{3+}/Tm^{3+} doped materials, the sensitizers of the excitation light are Yb^{3+} ions, and they also play the role of donor ions in every energy transfer process involved in the emission of visible and UV light (Figure 2(c)). Consequently, this quenching will be a relevant effect directly affecting the upconverted emissions.

It has been previously demonstrated[15] that due to the multiphoton intrinsic nature of the upconversion processes, blue and UV emissions from Tm^{3+} ions are generally favored by high Yb^{3+} contents, at least up to 20 mol. %. Then, for even larger concentrations, the upconverted intensities do not show any further increase, and in some cases, they can decrease. This fact is consistent with a strong quenching of the Yb^{3+} excited state caused by migration and the high surface/volume ratio of the nanoparticles, which would prevent Yb^{3+} ions from providing the needed energy to Tm^{3+} ions. Thus, from the point of view of the applications based on visible upconverted light, for higher Yb^{3+} concentrations it becomes more important to avoid quenchers by protecting the nanoparticles' surface.

IV. CONCLUSIONS

In conclusion, it has been proposed a simple method to quantify the IR energy transfer macroparameter in Yb^{3+}/Tm^{3+} co-doped samples, which is on the base of all the upconversion mechanisms involved in the emission of UV and blue light from Tm^{3+}. The obtained results indicate that in the nanoparticles $Yb^{3+} \rightarrow Tm^{3+}$ energy transfer parameter (K_1) shows the same value than in macroscopic crystals. This implies that the spectroscopic parameters involved, such as emission and absorption rates, remain unaltered when the material size is reduced, at least within the size range considered in this work. Nevertheless, lifetimes are much shorter in the nanoparticles than in macroscopic samples. It has been shown that this happens due to the high migration rate between Yb^{3+} ions and the strong contribution of surface defects in the case of nanoparticles. Both Yb^{3+} to Tm^{3+} infrared energy transfer parameter and Yb^{3+} to Yb^{3+} migration process have been characterized, allowing the construction of a single equation that describes Yb^{3+} lifetime for any Tm^{3+} and Yb^{3+} concentrations.

ACKNOWLEDGMENTS

The authors would like to acknowledge J. García Sevillano for his valuable assistance in IR luminescence measurements.

This work has been partially supported by the Spanish Ministerio de Ciencia e Innovación (MICINN) under Projects MAT2009-14102 (CRONOSOMATS) and MAT2011-23593, by Comunidad de Madrid (Project MICROSERES-CM (S2009/TIC-1476)), and by Junta de Andalucía (Grant FQM6090). N. O. Núñez also wants to thank MICINN and the Spanish Research Council (CSIC) for her financial support (PIE-200960I127), and M. Quintanilla would like to thank Fundación Ramón Areces for the postdoctoral program "Ciencias de la Vida y de la Material."

[1]A. Rapaport, J. Milliez, M. Bass, A. Cassanho, and H. Jenssen, J. Disp. Technol. **2**, 68 (2006).
[2]E. Downing, L. Hesselink, J. Ralston, and R. Macfarlane, Science **273**, 1185 (1996).
[3]L. F. Johnson and A. A. Ballman, J. Appl. Phys. **40**, 297 (1969).
[4]T. Hebert, R. Wannemacher, R. M. Macfarlane, and W. Lenth, Appl. Phys. Lett. **60**, 2592 (1992).
[5]R. Scheps, Prog. Quantum Electron. **20**, 271 (1996).
[6]S. F. Lim, R. Riehn, W. S. Ryu, N. Khanarian, C.-K. Tung, D. Tank, and R. H. Austin, Nano Lett. **6**, 169 (2006).
[7]D. K. Chatterjee, A. J. Rufaihah, and Y. Zhang, Biomaterials **29**, 937 (2008).
[8]Z. Tian, G. Y. Chen, X. Li, H. J. Liang, Y. S. Li, Z. G. Zhang, and Y. Tian, Lasers Med. Sci. **25**, 479 (2010).
[9]M. Gu, *Advanced Optical Imaging Theory, Optical Sciences* (Springer-Verlag, Berlín, 2000).
[10]F. Wang, W. B. Tan, Y. Zhang, X. P. Fan, and M. Q. Wang, Nanotechnology **17**, R1–R13 (2006).
[11]L. M. Maestro, E. M. Rodríguez, F. Vetrone, R. Naccache, H. L. Ramírez, D. Jaque, J. A. Capobianco, and J. García Solé, Opt. Express **18**, 23544 (2010).
[12]N. N. Dong, M. Pedroni, F. Piccinelli, G. Conti, A. Sbarbati, J. E. Ramírez-Hernández, L. M. Maestro, M. C. Iglesias-de la Cruz, F. Sanz-Rodríguez, A. Juarranz, F. Chen, F. Vetrone, J. A. Capobianco, J. G. Solé, M. Bettinelli, D. Jaque, and A. Speghini, ACS Nano **5**, 8665 (2011).
[13]G. F. Wang, W. P. Qin, L. L. Wang, G. D. Wei, P. Zhu, D. S. Zhang, and F. H. Ding, J. Rare Earths **27**, 330 (2009).
[14]C. Y. Cao, W. P. Qin, J. S. Zhang, Y. Wang, P. Zhu, G. F. Wang, G. D. Wei, L. L. Wang, and L. Z. Jin, J. Fluorine Chem. **129**, 204 (2008).
[15]M. Quintanilla, N. O. Núñez, E. Cantelar, M. Ocaña, and F. Cussó, Nanoscale **3**, 1046 (2011).
[16]G. De, W. P. Qin, J. S. Zhang, J. S. Zhang, Y. Wang, C. Y. Cao, and Y. Cui, J. Lumin. **122–123**, 128 (2007).
[17]D. Q. Chen, Y. S. Wang, Y. L. Yu, and P. Huang, Appl. Phys. Lett. **91**, 051920 (2007).
[18]G. F. Wang, W. P. Qin, G. D. Wei, L. L. Wang, P. Zhu, R. J. Kim, D. S. Zhang, F. H. Ding, and K. Z. Zheng, J. Fluorine Chem. **130**, 158 (2009).
[19]S. Schietinger, L. S. Menezes, B. Lauritzen, and O. Benson, Nano Lett. **9**, 2477 (2009).
[20]J. Shan, M. Uddi, R. Wei, N. Yao, and Y. G. Ju, J. Phys. Chem. C **114**, 2452 (2010).
[21]S. F. Lim, W. S. Ryu, and R. H. Austin, Opt. Express **18**, 2309 (2010).
[22]G. K. Liu, H. Z. Zhuang, and X. Y. Chen, Nano Lett. **2**, 535 (2002).
[23]G. K. Liu, X. Y. Chen, H. Z. Zhuang, S. Li, and R. S. Niedbala, J. Solid State Chem. **171**, 123 (2003).
[24]X. Y. Chen, H. Z. Zhuang, G. K. Liu, S. Li, and R. S. Niedbala, J. Appl. Phys. **94**, 5559 (2003).
[25]N. O. Núñez and M. Ocaña, Nanotechnology **18**, 455606 (2007).
[26]N. O. Núñez, M. Quintanilla, E. Cantelar, F. Cussó, and M. Ocaña, J. Nanopart. Res. **12**, 2553 (2010).
[27]F. W. Ostermayer, J. P. van der Ziel, H. M. Marcos, L. G. van Uitert, and J. E. Geusic, Phys. Rev. B **3**, 2698 (1971).
[28]F. Auzel, Compt. Rend. **263**, 819 (1966).
[29]S. Heer, K. Kömpe, H.-U. Güdel, and M. Haase, Adv. Mater. **16**, 2102 (2004).
[30]J. F. Suyver, J. Grimm, M. K. van Veen, D. Biner, K. W. Krämer, and H. U. Güdel, J. Lumin. **117**, 1 (2006).
[31]G. F. Wang, W. P. Qin, L. L. Wang, G. D. Wei, P. Zhu, and R. J. Kim, Opt. Express **16**, 11907 (2008).
[32]Y. Mita, T. Ide, M. Togashi, and H. Yamamoto, J. Appl. Phys. **85**, 4160 (1999).
[33]M. J. Weber, Phys. Rev. B **4**, 2932 (1971).
[34]J. W. Stouwdam, G. A. Hebbink, J. Huskens, and F. C. J. M. van Veggel, Chem. Mater. **15**, 4604 (2003).
[35]M. Inokuti and F. Hirayama, J. Chem. Phys. **43**, 1978 (1965).
[36]M. Yokota and O. Tanimoto, J. Phys. Soc. Jpn. **22**, 779 (1967).
[37]B. M. Tissue and B. Bihari, J. Fluoresc. **8**, 289 (1998).
[38]X. X. Cui, J. B. She, C. Gao, K. Cui, C. Q. Hou, W. Wei, and B. Peng, Chem. Phys. Lett. **494**, 60 (2010).
[39]T. T. Basiev and N. A. Glushkov, Opt. Mater. **32**, 1642 (2010).
[40]N. A. Glushkov, T. T. Basiev, and I. T. Basieva, JETP Lett. **93**, 697 (2011).
[41]B. Di Bartolo, in *Energy Transfer Processes in Condensed Matter*, edited by B. Di Bartolo (Plenum Press, New York, 1983), p. 156.
[42]C. Wyss, W. Lüthy, H. P. Weber, P. Rogin, and J. Hulliger, Opt. Commun. **144**, 31 (1997).
[43]D. F. de Sousa and L. A. O. Nunes, Phys. Rev. B **66**, 024207 (2002).
[44]T. Kushida, J. Phys. Soc. Jpn. **34**, 1318 (1973).